

Structured Low-Density Parity-Check Codes with Bandwidth Efficient Modulation

Michael K. Cheng, Dariush Divsalar, and Stephanie Duy*

Jet Propulsion Laboratory, California Institute of Technology, Pasadena, CA 91109-8099

ABSTRACT

In this work, we study the performance of structured Low-Density Parity-Check (LDPC) Codes together with bandwidth efficient modulations. We consider protograph-based LDPC codes that facilitate high-speed hardware implementations and have minimum distances that grow linearly with block sizes. We cover various higher-order modulations such as 8-PSK, 16-APSK, and 16-QAM. During demodulation, a demapper transforms the received in-phase and quadrature samples into reliability information that feeds the binary LDPC decoder. We will compare various low-complexity demappers and provide simulation results for assorted coded-modulation combinations on the additive white Gaussian noise and independent Rayleigh fading channels.

1. INTRODUCTION

The Jet Propulsion Laboratory (JPL) has been designing structured Low-Density Parity-Check (LDPC) Codes based on protographs and circulants.^{1,2} The JPL construction enables high-speed decoder implementations because the component protographs that are the building blocks to the bigger code graph can be decoded in parallel. The structure of the protograph then determines the threshold and error floor of the overall code. Divsalar et al.^{3,4} recognized that a protograph described by simple accumulate and repeat operators can yield codes with sharp waterfalls and low error floors. A family of accumulate repeat-by-4 jagged accumulate (AR4JA) LDPC codes was subsequently proposed for near-Earth and Deep-Space applications⁵ The family offers codes with rates of $1/2$, $2/3$, and $4/5$, and with information block lengths of 1024, 4096, and 16384 bits. Word error rate performance for the code family can be found in an IEEE Proceedings article by Andrews et al.²

The National Aeronautics and Space Administration (NASA) has established the Constellation project to build a next generation spacecraft to replace the aging Space Shuttle. Design for the Crew Exploration Vehicle (CEV) is underway to meet a scheduled launch date in 2014. Together with a new vehicle, NASA also plans to modernize its communications infrastructure and thereby, deploy modern coded-modulation schemes. The primary communications link for near-Earth manned missions is in the S-band and the bandwidth allocation is no more than 10 MHz wide with 6 MHz being the norm. This work explores various bandwidth efficient coded-modulation schemes suitable for high data rate near-Earth communications. More specifically, we take 8-PSK, 16-APSK, and 16-QAM modulations in different combinations with high rate LDPC codes and compare these performances first on the additive white Gaussian channel (AWGN), then on the independent Rayleigh fading channel. The independent Rayleigh fading model also can be used with a channel interleaver where multiple codeword frames are interleaved prior to modulation. We show that proper demodulation and decoding of bandwidth efficient coded-modulation can approach Channel Capacity. This paper is organized as follows. In Section 2, we provide a brief description of the AR4JA LDPC code family. LDPC belief propagation decoders take as input soft symbol information. In Section 3, we derive the expressions to compute the exact log likelihood ratios (LLRs) of the demodulated soft symbols for each modulation scheme. We also provide simple low-complexity approximations to the exact expressions that would incur only a small performance penalty. In Section 4, we describe modeling of independent Rayleigh fading. In Section 5 we catalog the performances of various coded-modulation schemes on the AWGN and the independent Rayleigh fading channel. In Section 6, we close this paper with a few remarks.

*Stephanie Duy was a summer intern at JPL from May-August, 2008 and is currently an undergraduate senior in the Department of Electrical and Computer Engineering at the University of Maine

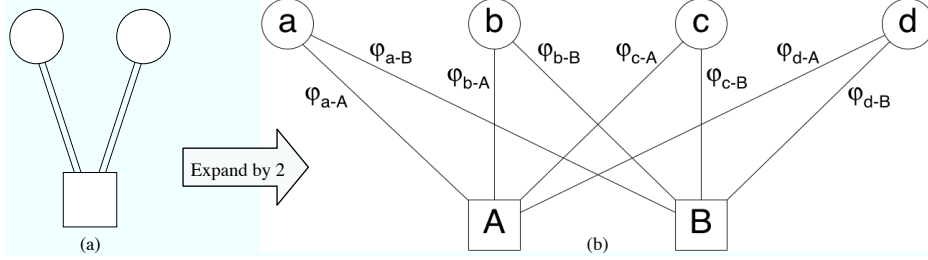


Figure 1. (a) A regular (2, 4) protograph. (b) Expand protograph by 2 to eliminate parallel edges.

2. THE FAMILY OF AR4JA LDPC CODES

A protograph is a bi-partite graph with a relatively small number of nodes. The AR4JA LDPC code is built by making copies of a protograph and permuting the connecting edges. As an example, a simple (2, 4) regular protograph and the “copy-and-permute” operation are illustrated in Fig. 1. Each component protograph of a larger code can be treated by an independent decoding circuit. Therefore, this construction facilitates parallel hardware implementation and enables a high speed decoder realization. Moreover, the AR4JA design also ensures that the code’s minimum distance grows linearly with the block size.^{3,6} The result is a family of codes that exhibit very low error floors.

Decoding of binary LDPC codes iteratively refines the symbol reliabilities expressed in LLRs until all parity checks are satisfied or a iteration limit is reached. An accurate computation of the LLRs is therefore key to optimizing decoder performance and the derivation of the LLRs depend on the particular modulation scheme.

3. LDPC CODED-MODULATION

For binary coded-modulation schemes, channel symbols are demodulated by calculating the LLRs of the bits that comprise a modulation symbol. A bit-wise LLR is the log ratio of the probability that a bit is 0 to the probability that a bit is 1 conditioned on the channel observations. On the binary AWGN channel with BPSK and QPSK transmissions, the LLR for each channel symbol is simply the channel observation scaled by $2A/\sigma^2$, from here on referred to as the scaling factor. The signal amplitude is A and the AWGN noise variance is σ^2 . In this Section, we provide demapping function that transforms the received in-phase and quadrature samples into bit-wise LLRs for each bandwidth efficient modulation.

3.1 8-Phase Shift Keying (PSK)

In 8-PSK modulation, we consider a constellation with Gray code mapping where each neighboring 8-PSK symbol on the modulation circle differs by one bit in the bit-to-symbol mapping. Therefore, the 8-PSK constellation symbol in a counter clockwise direction would map to the bits [000, 001, 011, 010, 110, 111, 101, 100]. We derive the bit LLR for each of the three bits representing the modulation phases. Let the received in-phase and quadrature signal samples at the output of the matched filter after the AWGN channel be represented as:

$$I = A \cdot \cos\phi + n_I \quad (1)$$

$$Q = A \cdot \sin\phi + n_Q. \quad (2)$$

The modulation phase ϕ can be represented by $\phi(b_2, b_1, b_0)$ which shows the dependency on the three bits b_2, b_1 , and b_0 , where b_2 is the MSB and b_0 is the LSB. The phase ϕ takes on the following values:

$$\phi = \frac{(2i + 1)\pi}{8}, \quad i = 0, 1, \dots, 7. \quad (3)$$

Let λ_j represent the LLR for bit b_j , $j = 0, 1, 2$, then we apply the Euclidean distance metric in the LLR computation to arrive at

$$\lambda_j = \ln \frac{\sum_{b_2, b_1, b_0: b_j=0} \exp\left(\frac{-1}{2\sigma^2} \left((I - A \cdot \cos\phi(b_2, b_1, b_0))^2 + (Q - A \cdot \sin\phi(b_2, b_1, b_0))^2 \right)\right)}{\sum_{b_2, b_1, b_0: b_j=1} \exp\left(\frac{-1}{2\sigma^2} \left((I - A \cdot \cos\phi(b_2, b_1, b_0))^2 + (Q - A \cdot \sin\phi(b_2, b_1, b_0))^2 \right)\right)}$$

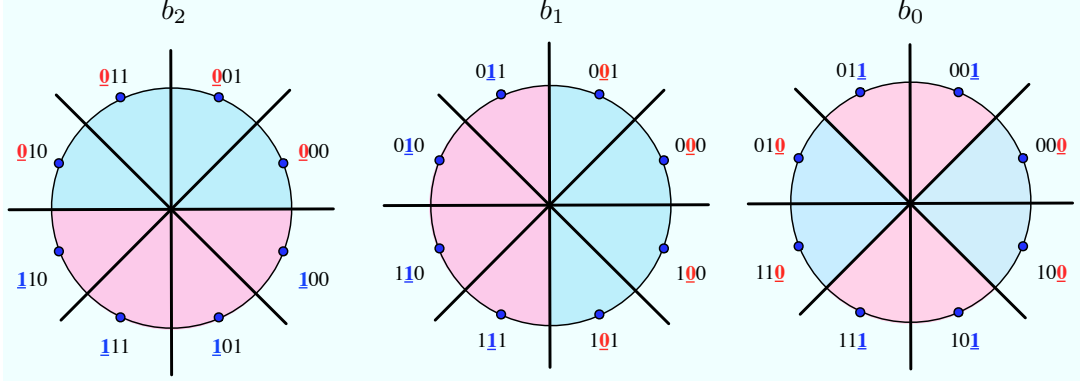


Figure 2. Low-complexity LLR approximation for 8-PSK.

$$= \ln \frac{\sum_{b_2, b_1, b_0: b_j=0} \exp\left(\frac{A}{\sigma^2} (I \cdot \cos \phi(b_2, b_1 b_0) + Q \cdot \cos \phi(b_2, b_1 b_0))\right)}{\sum_{b_2, b_1, b_0: b_j=1} \exp\left(\frac{A}{\sigma^2} (I \cdot \cos \phi(b_2, b_1 b_0) + Q \cdot \cos \phi(b_2, b_1 b_0))\right)}. \quad (4)$$

Note that in (4) the maximum term in the summation generally dominates over other terms in the summation. Therefore, equation (4) can be closely approximated by

$$\lambda_j = \frac{A}{\sigma^2} \left(\max_{b_2, b_1, b_0: b_j=0} \{I \cdot \cos \phi(b_2, b_1 b_0) + Q \cdot \cos \phi(b_2, b_1 b_0)\} - \max_{b_2, b_1, b_0: b_j=1} \{I \cdot \cos \phi(b_2, b_1 b_0) + Q \cdot \cos \phi(b_2, b_1 b_0)\} \right). \quad (5)$$

We shall refer to this simplified LLR computation as “approximation method 1.”

We can further reduce the approximation of the LLR for the Gray code mapping to a simpler expression without the log or even the max operation. Take a look at Fig. 2. The boundary for the MSB being a bit 0 or a bit 1 lies on the horizontal axis. That is, if the quadrature component of the received symbol is greater than zero, it is likely that the transmitted symbol is one of the four symbols in the top half circle with the MSB 0. The LLR for the MSB here should be greater than zero like the quadrature component. Otherwise, the quadrature component of the received symbol is less than zero. The transmitted symbol is likely one of the four symbols in the bottom half circle with the MSB 1. The LLR for the MSB here should be less than zero again like the quadrature component. The confidence of the LLR is also proportional to the scaling factor given by the ratio of the signal amplitude to the noise variance A/σ^2 . The middle bit has a similar derivation. Except in this case, the middle bit 0 or 1 boundary is the vertical axis. If the in-phase component is greater than zero, then the middle bit is likely a 0 and the LLR should be positive. Otherwise, the middle bit is likely a 1 and the LLR should be negative. The observation for the LSB is a little different. If the magnitude of the in-phase component is larger than the magnitude of the quadrature component (indicated by the two horizontal pies), the LSB is likely a 0 and the LLR should be positive. Otherwise, the quadrature component is larger than the in-phase component (indicated by the vertical pies), the LSB is likely a 1 and the LLR should be negative. In all cases, the LLR is proportional to the scaling factor A/σ^2 . More specifically we have

$$\lambda_2 = \alpha \frac{A}{\sigma^2} Q \quad (6)$$

$$\lambda_1 = \alpha \frac{A}{\sigma^2} I \quad (7)$$

$$\lambda_0 = \beta \frac{A}{\sigma^2} (|I| - |Q|). \quad (8)$$

The constants α and β are numbers selected through simulations. Our results show that the best performance is obtained when $\alpha = 1/\sqrt{2}$ and $\beta = 1/\sqrt{2}$ respectively. We shall refer to this simplified LLR computation as “approximation method 2.” We will compare the performance of the three expressions in Section 5.

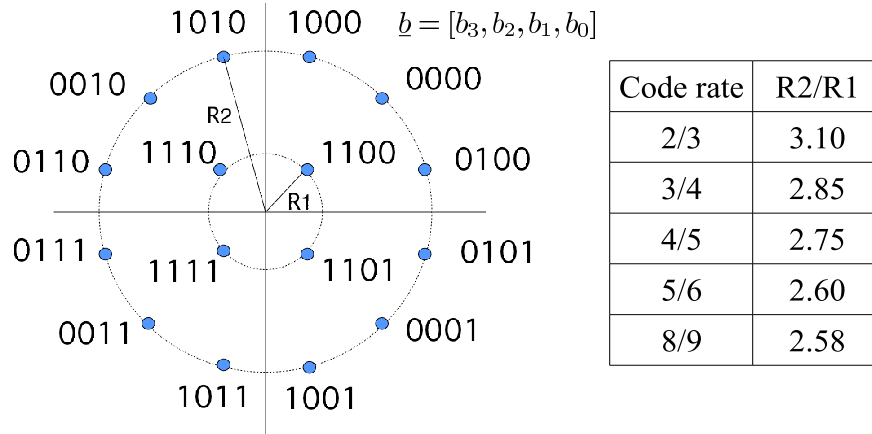


Figure 3. 16-APSK modulation with Gray mapping. The ratio of the radii is selected to maximize the Capacity of the coded-modulation for each code rate.

3.2 16-Amplitude Phase Shift Keying (APSK)

If a higher spectral efficiency is desired, a larger Constellation can be used. Consider a 16-APSK modulation with Gray code mapping as shown in Fig. 3. The symbols are spread across two concentric circles with two radii R_2 and R_1 . The ratio of the radii can be selected to maximize the coded-modulation capacity. The table in Fig. 3 gives the proper ratio of R_2/R_1 for some commonly used code rates.

For each channel observation the in-phase and quadrature components are defined as

$$I = A_b \cdot \cos \phi + n_I \quad (9)$$

$$Q = A_b \cdot \sin \phi + n_Q \quad (10)$$

where A_b is either R_1 or R_2 . To derive the bit-wise LLR for 16-APSK, we again use the Euclidean distance metric. We have to however, take into account that there are two possible amplitudes for the modulated symbols. Let λ_j represent the LLR for bit b_j , $j = 0, 1, 2, 3$, we have

$$\begin{aligned} \lambda_j &= \ln \frac{\sum_{b_3, b_2, b_1, b_0: b_j=0} \exp\left(\frac{-1}{2\sigma^2} \left((I - A_b \cdot \cos \phi(b_2, b_1 b_0))^2 + (Q - A_b \cdot \sin \phi(b_2, b_1 b_0))^2 \right)\right)}{\sum_{b_3, b_2, b_1, b_0: b_j=1} \exp\left(\frac{-1}{2\sigma^2} \left((I - A_b \cdot \cos \phi(b_2, b_1 b_0))^2 + (Q - A_b \cdot \sin \phi(b_2, b_1 b_0))^2 \right)\right)} \\ &= \ln \frac{\sum_{b_3, b_2, b_1, b_0: b_j=0} \exp\left(\frac{A_b}{\sigma^2} \left(I \cdot \cos \phi(b_2, b_1 b_0) + Q \cdot \sin \phi(b_2, b_1 b_0) - \frac{A_b}{2} \right)\right)}{\sum_{b_3, b_2, b_1, b_0: b_j=1} \exp\left(\frac{A_b}{\sigma^2} \left(I \cdot \cos \phi(b_2, b_1 b_0) + Q \cdot \sin \phi(b_2, b_1 b_0) - \frac{A_b}{2} \right)\right)}. \end{aligned} \quad (11)$$

Here A_b is either R_1 or R_2 depending on the position of the modulation symbol represented by $[b_3, b_2, b_1, b_0]$. Like before, the maximum term in the summation generally dominates over other terms in the summation. And equation (11) can be closely approximated by

$$\lambda_j = \frac{A_b}{\sigma^2} \left(\max_{b_3, b_2, b_1, b_0: b_j=0} \{I \cdot \cos \phi(b_2, b_1 b_0) + Q \cdot \sin \phi(b_2, b_1 b_0)\} - \max_{b_3, b_2, b_1, b_0: b_j=1} \{I \cdot \cos \phi(b_2, b_1 b_0) + Q \cdot \sin \phi(b_2, b_1 b_0)\} \right). \quad (12)$$

3.3 16-Quadrature Amplitude Modulation (QAM)

We can label a 16-QAM constellation using Gray code mapping by treating each dimension separately as illustrated in Fig. 4. The distance between any two adjacent symbols in the in-phase or the quadrature direction

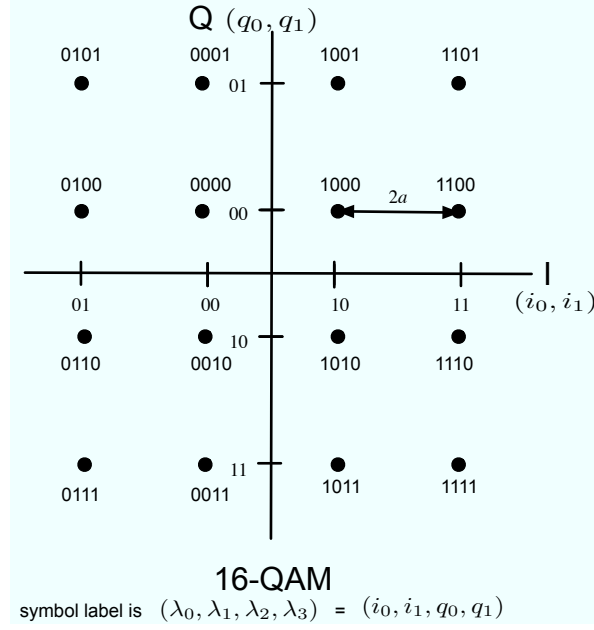


Figure 4. 16-QAM with Gray code mapping.

is $2a$ and therefore, the minimum distance of the 16-QAM constellation is $d = 2a$. The average power of the 16-QAM constellation is

$$\begin{aligned}
 p &= \frac{1}{4}(a^2 + a^2) + \frac{1}{2}((3a)^2 + a^2) + \frac{1}{4}((3a)^2 + (3a)^2) \\
 &= 10a^2.
 \end{aligned} \tag{13}$$

Thus, the minimum distance as a function of transmitted power is $d = \sqrt{\frac{4p}{10}}$ and with unit power, $d = 2/\sqrt{10}$. We can again apply the Euclidean distance metric in the exact computation of the symbol LLRs for 16-QAM similar to (11) where $A_b = a\sqrt{2}, a\sqrt{10},$ or $3a\sqrt{2}$ depending on the constellation point. We could also estimate the LLR expression using again a reasoning similar to one applied in deriving the 8-PSK approximation 2 expression without the need to compute exponential of large numbers. For each of the bit positions, we can compute the 16-QAM LLR as

$$\lambda_0 = \alpha I \tag{14}$$

$$\lambda_1 = \beta(d - |I|) \tag{15}$$

$$\lambda_2 = \alpha Q \tag{16}$$

$$\lambda_3 = \beta(d - |Q|) \tag{17}$$

where α and β are again chosen empirically from simulation results and should be a function of the average power of the constellation and the AWGN noise variance.

4. INDEPENDENT RAYLEIGH FADING CHANNEL

To model independent Rayleigh fading, we take our complex signal $Ae^{-j\phi}$ and multiply it with a random Rayleigh distributed variable ρ generated by summing together two independent Standard Normal random variables. More specifically,

$$\rho = \sqrt{\frac{x_1^2 + x_2^2}{2}} \tag{18}$$

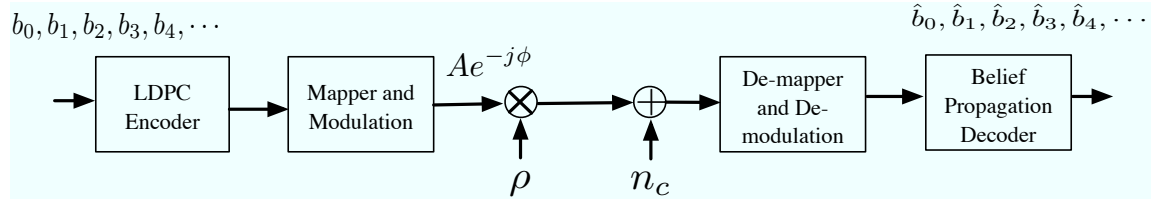


Figure 5. System model for bandwidth efficient LDPC coded-modulation.

where $x_1, x_2 \sim \eta(0, 1)$ are Gaussian random variables with zero mean and unit variance. The variance of ρ is normalized to

$$E[\rho^2] = \frac{1}{2} (E[x_1^2] + E[x_2^2]) = 1. \quad (19)$$

Therefore, we do not have to re-normalize the SNR for our simulation results in the Rayleigh fading case. The in-phase and quadrature channel observations become

$$I = A\rho \cdot \cos \phi + n_I \quad (20)$$

$$Q = A\rho \cdot \sin \phi + n_Q. \quad (21)$$

At the receiver, we assume perfect channel state information and thus, perfect knowledge of ρ for each symbol out of the matched filter. To compute the symbol LLRs in the presence of independent Rayleigh fading, we simply apply the knowledge of ρ in the same expressions derived earlier. In the 8-PSK case, we substitute $A\rho$ for A in equations (4) - (8). In the 16-APSK case, we substitute $A_b\rho$ for A_b in equations (11) and (12). In the 16-QAM case, we multiply the observations I and Q by ρ to get $\lambda_0 = \alpha\rho I$ and $\lambda_2 = \alpha\rho Q$. We also multiply d by ρ to get $\lambda_1 = \rho(\rho d - |I|)$ and $\lambda_3 = \rho(\rho d - |Q|)$. An illustration of our system model is given in Fig. 5.

5. PERFORMANCE

We catalog the simulated performance of various coded-modulation techniques discussed in this paper. We also measure the penalty for the low-complexity LLR approximations presented earlier in Section 3.1.

5.1 AR4JA (1280,1024) LDPC Coded-Modulation with 8-PSK

5.1.1 AWGN Channel

We compare the performances of LLR computations using the exact expression, approximation 1, and approximation 2 for AR4JA (1280,1024) LDPC coded-modulation with 8-PSK on the additive white Gaussian channel (AWGN) in Fig. 6(a). Again the exact expression is given by (4), approximation 1 is given by (5), and approximation 2 is given by (6) - (8). Looking at the zoomed-in plot of Fig. 6(b), we see that the “max” approximation (or approximation 1) does not incur any additional penalty on the coded-modulation performance. The approximation 1 curve is nearly identical to the curve obtained with the exact LLR expression with variation rooted only in the monte-carlo nature of the generated random noise. The penalty of approximation 2 is less than 0.1 dB in signal-to-noise (SNR) ratio. By giving up this small coding gain, we can avoid the need to take the maximum of various arguments or compute the exponential of large numbers. The complexity reduction of approximation 2 is evident even in our experiments since we are able to simulate to a lower error rate using approximation 2 than using approximation 1 or the exact LLR computation as seen in Fig. 6(a).

5.1.2 Independent Rayleigh Fading Channel

We repeat the simulations on the independent Rayleigh fading channel. Since we observed that LLR computation using approximation 1 generated a result nearly identical to the exact LLR computation in Section 5.1.1, we only collect results using approximation 1 and approximation 2 for the Rayleigh scenario. The curves are given in Fig. 7(a). Notice again that the penalty of approximation 2 to approximation 1 is only 0.1 dB and the savings in computation makes approximation 2 an attractive alternative to computing the exact LLR. We compare the performance of this code-modulation combination on the independent Rayleigh channel to that measured on the AWGN channel in Fig. 7(b) and observe an SNR gap of about 5 dB. The uncoded 8-PSK capacity gap between AWGN and Rayleigh is around 4 dB so our coded-modulation gap is about 1 dB larger.

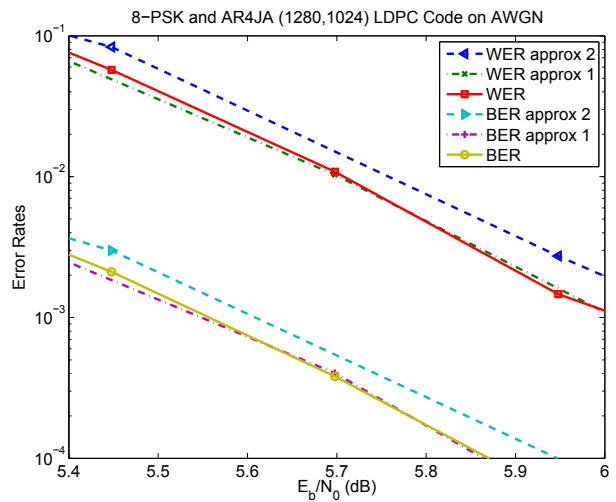
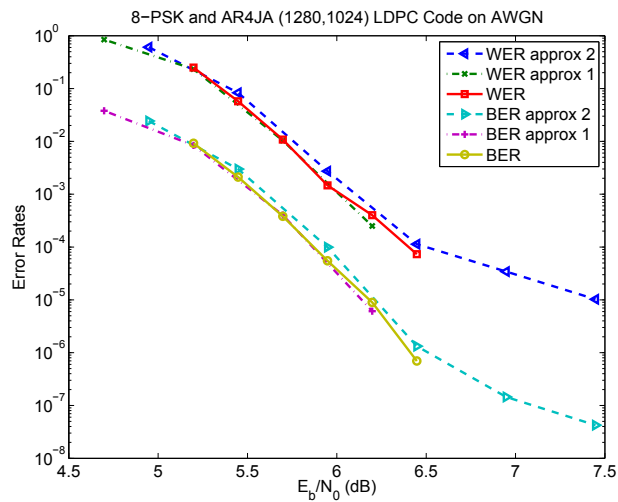


Figure 6. (a) AR4JA (1280,1024) LDPC coded-modulation with 8-PSK on AWGN (b) Zoomed-in

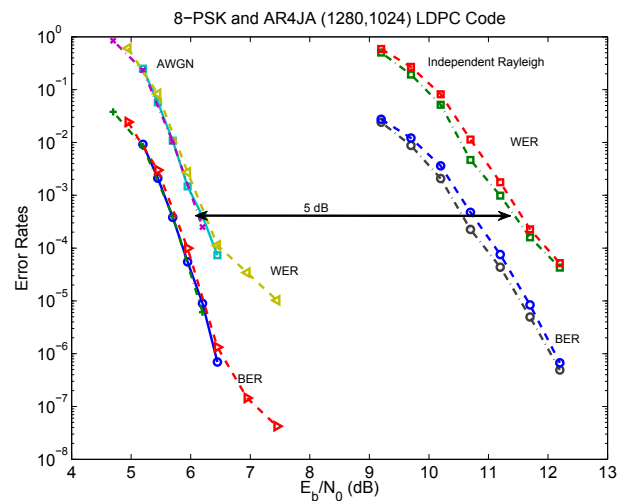
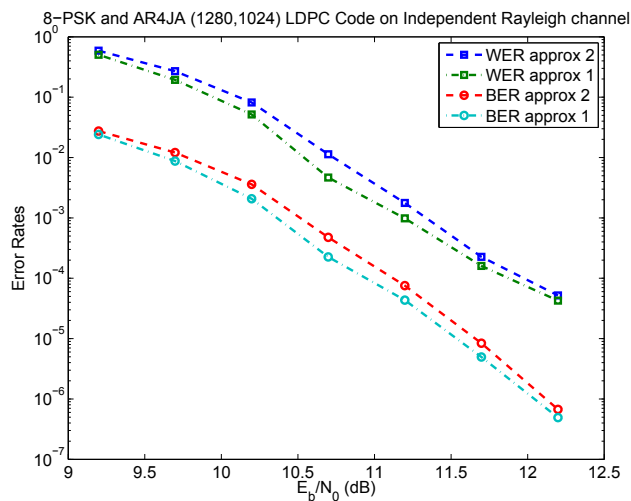


Figure 7. (a) AR4JA (1280,1024) LDPC coded-modulation with 8-PSK on the independent Rayleigh fading channel (b) Performance gap between AWGN and Rayleigh

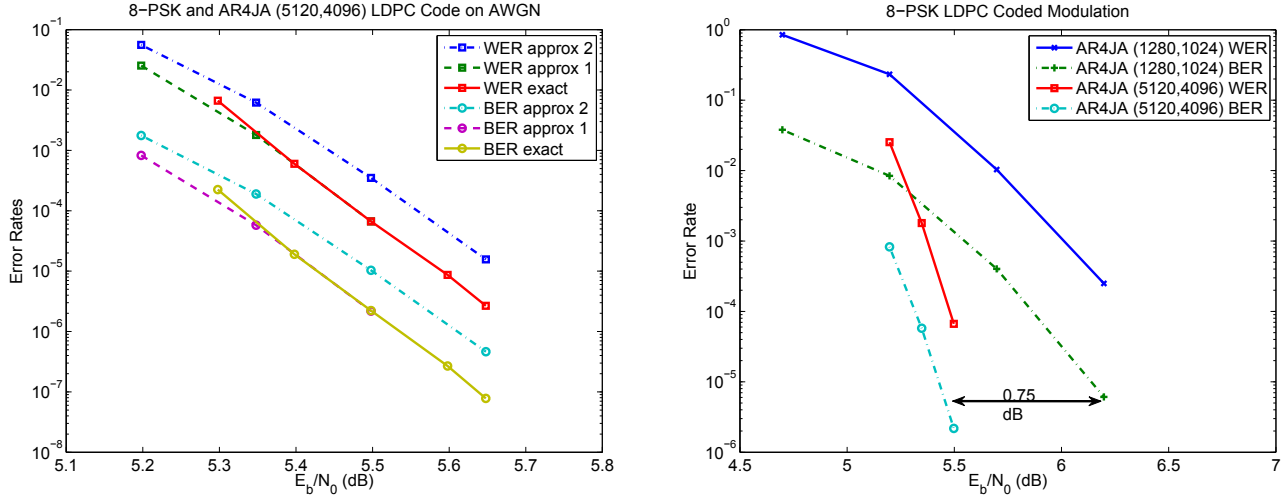


Figure 8. (a) AR4JA (5120,4096) LDPC coded-modulation with 8-PSK on the AWGN channel (b) Performance gain in using a longer block code

5.2 AR4JA (5120,4096) LDPC Coded-Modulation with 8-PSK

5.2.1 AWGN Channel

We provide the performance of the AR4JA (5120,4096) coded-modulation with 8-PSK in Fig. 8(a) and compare the result with the shorter AR4JA (1280,1024) code in Fig. 8(b). First, the error rate performance measured using the approximations for this longer LDPC code agrees with the penalty of the short code. That is, approximation 1 produced a result nearly identical to computing the exact LLR while approximation 2 only incurred an extra 0.1 dB SNR gap. If latency is not an issue, a longer code can be used to obtain an additional coding gain. Latency is typically dominated by the time required to collect a codeword length of bits. Therefore, latency should not be a concern on Mbps high data rate links where the buffering delay even for the AR4JA (5120,4096) code is only on the order of *usecs* especially when an extra 3/4 dB of coding gain can be had by simply using a longer code in the same family. Also note that the longer LDPC code offers a sharper waterfall region where the error rate falls faster with increasing SNR values as seen in Fig. 8(b).

5.2.2 Independent Rayleigh Fading Channel

We repeat the simulations of the AR4JA (5120,4096) coded-modulation with 8-PSK on the independent Rayleigh fading channel and plot the results in Fig. 9(a). We do not compute the LLRs exactly and only apply the approximations to save simulation time. As before, approximation 2 only leads to a 0.1 dB penalty when compared to approximation 1. We compare the Rayleigh performance to the AWGN performance and observe a 4.5 dB SNR gap as illustrated in Fig. 9(b).

5.3 AR4JA (5120,4096) LDPC Coded-Modulation with 16-APSK

We plot the performance of extremely bandwidth efficient LDPC coded modulation with the AR4JA (5120,4096) LDPC code and 16-APSK in Fig. 10(a). We can only apply approximation 1 here since approximation 2 is derived only for Gray mapped 8-PSK. The gap between the AWGN channel and the independent Rayleigh fading channel is about 4.2 dB. We compare various combinations of bandwidth efficient LDPC coded-modulations in Fig. 10(b). As a benchmark, we also included the simulated performance of the C2 LDPC code. The C2 code is a quasi-cyclic LDPC code with a base parameter (8176,7156).⁵ So at a code rate of 7/8th, the code offers a better bandwidth efficiency than the rate 4/5th AR4JA (5120,4096) code but at reduced coding gain (about 3/4 dB less). The C2 code is also 60% longer in length and therefore incurs this additional latency.

If both bandwidth and power are important, an effective coded-modulation combination would be 16-APSK with AR4JA (5120,4096) LDPC code since this scheme offers a spectral efficiency of 3.2 bits/sec/Hz at a required operating SNR that is even less than the 8-PSK C2 combination with a spectral efficiency of 2.625 bits/sec/Hz.

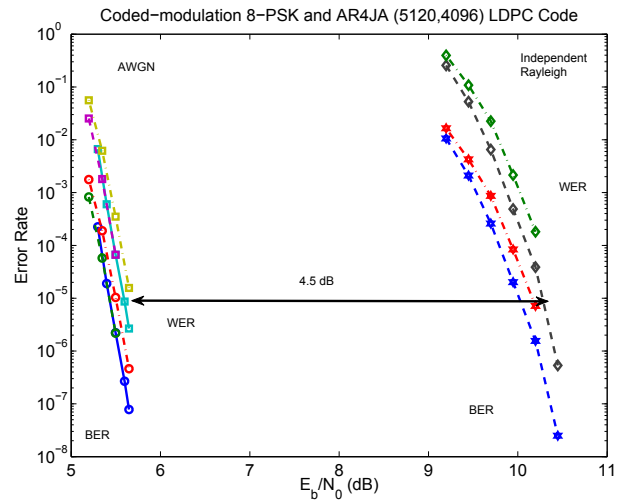
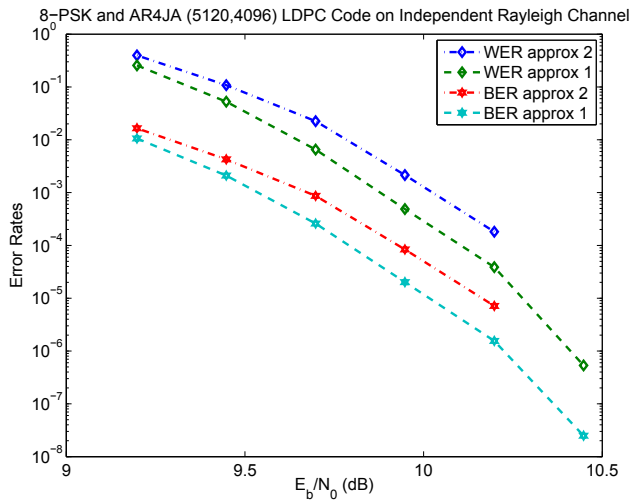


Figure 9. (a) AR4JA (5120,4096) LDPC coded-modulation with 8-PSK on the independent Rayleigh fading channel (b) Performance gap between AWGN and Rayleigh

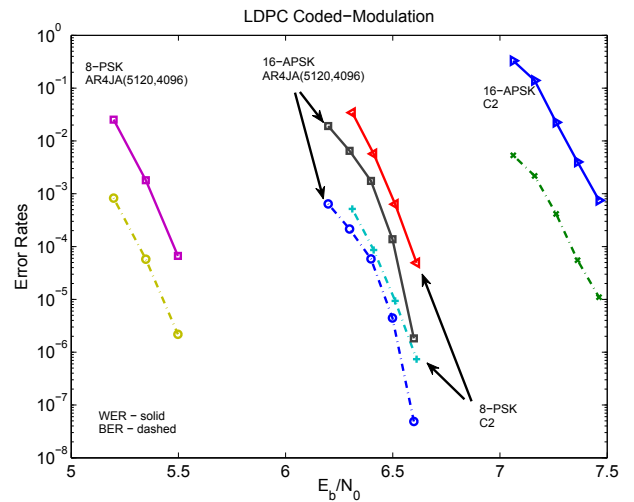
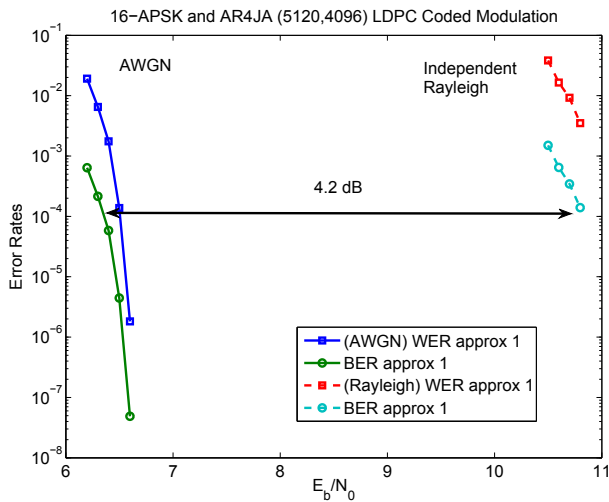


Figure 10. (a) AR4JA (5120,4096) LDPC coded-modulation with 16-APSK (b) Different coded-modulation combinations

6. SUMMARY

In this work we presented various LDPC coded-modulation schemes for bandwidth efficient communications with a focus on the JPL family of AR4JA LDPC codes that is designed with minimum distance that grows linearly with block length. We demonstrated through simulation that the structured AR4JA codes can be combined with higher-order modulations to achieve a good balance between power and spectral efficiency and in most cases the combined coded-modulation would operate within 1 dB of Capacity. We also gave low-complexity expressions to compute the soft symbol reliabilities for input to the LDPC decoders. These approximations reduces the computation requirement and allows these coded-modulations schemes to be used in practice. We cataloged the performance of many practical bandwidth efficient coded-modulation combinations for reference.

ACKNOWLEDGMENTS

This research was carried out at the Jet Propulsion Laboratory, California Institute of Technology, and was sponsored by the National Aeronautics and Space Administration.

References

- [1] J. Thorpe, "Low-Density Parity-Check Codes Constructed from Protographs," *JPL Interplanetary Network Progress Report 42-154*, Aug. 2003.
- [2] K. S. Andrews, D. Divsalar, S. Dolinar, J. Hamkins, C. R. Jones, and F. Pollara, "The development of Turbo and LDPC codes for deep-space applications," *Proc. of the IEEE* **95**, pp. 2142–2156, Dec. 2007. Special Issue on Tech. Adv. in Deep Space Comm. and Tracking: Part 2.
- [3] D. Divsalar, C. Jones, S. Dolinar, and J. Thorpe, "Protograph based LDPC codes with minimum distance linearly growing with block size," in *Proc. IEEE Global Telecom. Conf.*, (St. Louis, MO, USA), Nov. 2005.
- [4] D. Divsalar, S. Dolinar, and C. Jones, "Construction of protograph LDPC codes with linear minimum distance," in *Proc. IEEE Int. Symp. Information Theory*, (Seattle, WA, USA), June 2006.
- [5] CCSDS, "Low-Density Parity-Check Codes for Use in Near-Earth and Deep Space." Consultative Committee for Space Data Systems Standard, 131.1-O-2, Sept. 2007. Orange Book.
- [6] A. Abbasfar, D. Divsalar, and J. Yao, "Accumulate and repeat accumulate coded modulation," in *Proc. IEEE Military Commun. Conf.*, (Monterey, CA), Oct. 2004.